

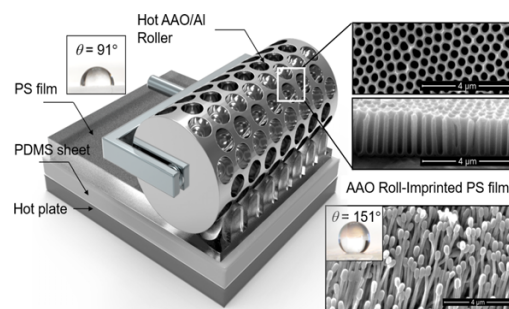
Water Repellency of Large-Scale Imprinting-Assisted Polymer Films

Harim Choi¹
Seulyi Lee¹
Sang Hee Park²
Joong Se Ko¹
Hoichang Yang^{*1}

¹Department of Applied Organic Materials Engineering, Inha University, Incheon 22212, Korea
²Department of Chemical and Biological Engineering, Korea University, Seoul 02841, Korea

Received March 30, 2017 / Revised May 3, 2017 / Accepted May 4, 2017

Abstract: We report that the water repellency of polymeric film surfaces can be simply tuned by pressing softened polymer films into porous anodized aluminum oxide (AAO) templates. Highly-dense nano-pillars and nano-hairs on the polymer surfaces are reproduced *via* physically or chemically separating the AAO templates from the impressed polymer films. The resulting polymeric nano-textures show various aspect ratios (ARs) between height and cross-sectional diameter (from 2 to 130), depending on the viscoelastic response of the polymer chains during hot AAO pressing and the subsequent separation procedures. The water contact angle values on the nano-textured polymer films considerably changed from 91° to 160° with an increase in AR. Using hot pressing and physical detachment of a porous AAO-covered Al cylinder roller, we successfully demonstrated the potential for large-area fabrication of superhydrophobic polymer films with characteristics that are similar to lotus leaves.



Keywords: superhydrophobicity, texturing, wettability, contact angle, aluminum oxide (AAO).

1. Introduction

Many creatures in nature possess near perfect structures and properties, exhibiting harmonization and unification between their structure and function. Lotus leaves are recognized as an ideal model of engineered self-cleaning. Artificial mimicry of these superhydrophobic surfaces has been an attractive goal in various industrial fields in order to remove undesirable contaminants from the surfaces of high-end products.¹⁻⁴ Superhydrophobicity is generally defined as a surface that produces a static water contact angle (WCA) greater than 150°. Such a high WCA on a material surface cannot be achieved without geometrical supports such as periodic microscale objects, nanoscale objects, or their mixtures.⁵ Thus, most superhydrophobic surfaces contain nanometer- or micrometer-scaled profiles of low-surface energy (γ) materials.⁶

Fractal surface nanostructures of hydrophobic materials drastically increase the WCAs on nano-textured surfaces. Additionally, microscale surface texturing of hydrophobic materials, with an average interval spacing ranging from a few to a hundred μm , has been shown to improve a material's surface hydrophobicity.^{7,8} Different wetting states and contact angle hysteresis behavior of water drops are possible for various hydrophobic surfaces, depending on the materials and surface geometries. These include the following states: (1) Wenzel (when water drop-

lets adsorb to a surface in a wet-contact mode),⁹ (2) Cassie-Baxter (CB) (when water droplets adopt a non-wet-contact mode),¹⁰ (3) "Lotus" state (a special case of the CB state),¹¹⁻¹³ and (4) a transition between Wenzel and CB (most practical samples).¹⁴

Among the various surface-texturing methods for soft materials,^{3,15-17} hot pressing (or imprinting) polymer layers using porous anodized aluminum oxide (AAO) templates is especially effective.¹⁸⁻²⁰ In this method, the geometries of the nano-pillars formed on the pressed polymer surfaces are controlled using AAO molds, which have controllable nanopores with a specific average pore diameter (D_p), height (H_p), and interpore distance (D_{inter}). However, the shape and aspect ratio (AR, ratio of domain height to diameter) effects of the polymeric domains on the water repellency of textured films have not been systematically studied for samples with consistent spacing between polymeric domains.

Here, we demonstrated a facile and highly efficient nano-texturing method for polymer films, which can contain various nano-textures (*e.g.*, rods, piles, spikes, and hairs), by (1) hot pressing with a nano-porous AAO template ($D_p=200$ nm, $D_{inter}=500$ nm, and $H_p=1.6$ μm) and (2) chemically or physically separating the polymer-AAO interface. The treated films contained various textured skin layers, including vertically-standing nano-domains (with an average interval of about 500 nm), showing a wide range ARs between 2 and 130. The WCA on textured polystyrene (PS) films dramatically increased from 91° (on the flat surface) to 160° (on the hairy PS skin layer). In addition, the tendency for water repellency was reproduced on other polymer systems. By using a similar film pressing and physical detachment method with a circular AAO layer on an Al cylinder, we successfully fabricated a one-pot large-area nano-textured PS film, thereby demonstrating the potential for large-area fabrication of superhydrophobic

Acknowledgments: This work was supported by grants from the Ministry of Trade, Industry & Energy (MOTIE, Korea) under Industrial Technology Innovation Program (10062082) and the Industrial Fundamental Technology Development Program (10052893).

***Corresponding Author:** Hoichang Yang (hcyang@inha.ac.kr)

polymer films that behave similarly to lotus leaves.

2. Experimental

2.1. Materials, polymer films, and AAO fabrication

All acids and solvents were purchased from Aldrich and were used without further purification. Polystyrene (PS, molecular weight, $M_w=100$ kDa, Aldrich) was compression-molded, and the film thicknesses were between 250 and 300 μm . Highly-purified Al sheets (99.999%, Goodfellow, 3×5 cm^2 and a thickness of 1 mm) and cylinders were used for Al anodization.

Flat and circular AAO templates for the surface-texturing process of polymer films were prepared by the following steps: (1) Al electro-polishing, (2) anodization of Al, (3) AAO etching, (4) dimension-controlled anodization of Al, and (5) AAO etching (or pore widening).²¹⁻²³ The surface textures observed after each step are schematically presented in Figure 1. First, highly purified Al sheets were electrochemically polished at a constant current in an electrolyte containing perchloric acid and ethanol (1:4 by volume) at 7 $^\circ\text{C}$ (Figure 1(b)). Porous AAO layers on either the Al sheet or cylinder were formed on the electro-polished Al surface by sequential procedures (Figures 1(c)-(e)). The first step of the anodization of Al was conducted in a 0.1 M aqueous solution of phosphoric acid (85% H_3PO_4 , Aldrich) at 195 V and 0 $^\circ\text{C}$ for 24 h. Then, the resulting AAO layer was dissolved from the anodized

Al sample inside an aqueous etchant, which contained 1.8 wt% chromic acid (H_2CrO_4) and 6 wt% H_3PO_4 , at 60 $^\circ\text{C}$ overnight. The second anodization of Al was performed under the same conditions as the first, except that the anodization time (t) was determined based on the t -dependent H_p empirical formula (see Figure S1(a) in the Supporting Information, SI). Then, the vertical nanopores inside the AAO layers were etched in a 0.1 M H_3PO_4 solution at 30 $^\circ\text{C}$, until their D_p reached approximately 200 nm (Figure S1(b) in the SI). Finally, some of the AAO surfaces were modified to be hydrophobic using octadecyltrichlorosilane (ODTS, 97%, Aldrich) as a self-assembly monolayer (SAM) monomer. The UV- O_3 -treated AAO samples were SAM-treated inside a chamber with vapor-phase ODTS at 150 $^\circ\text{C}$ for 1 h and then rinsed several times with excess toluene to yield an ODTS-coupled AAO surface (Figure 1(f)).

2.2. Preparation of surface-textured polymer films

Surface-texturing methods of polymer films can be used to produce various nanostructures on the topmost skin layers, as illustrated in Figure 2. First, a compression-molded polymer film was placed on an AAO template sheet that was kept at a specific processing temperature (T_p was greater than the glass transition temperature, T_g of the polymers used in this study, Figure S2 in SI) inside an N_2 -purged heating chamber with a pressure-controllable vacuum unit (Figure 2(a)). The degree of polymer filling

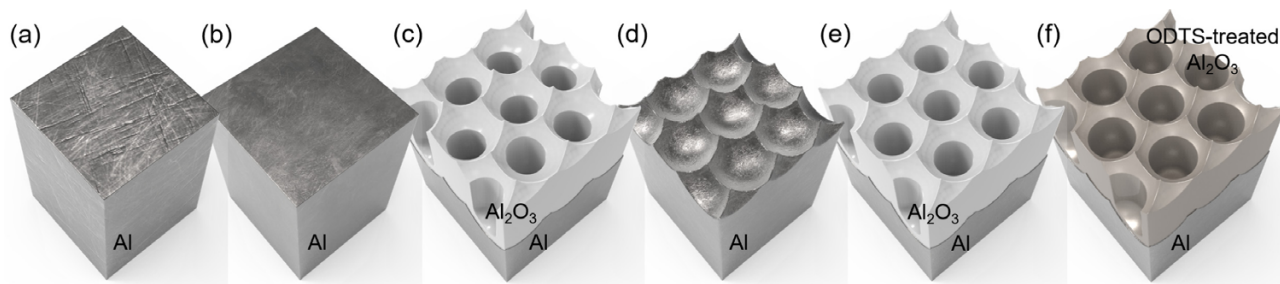


Figure 1. Schematic illustration of the Al surfaces (a) before and (b-e) after each fabrication step: (b) electro-polishing, (c) anodization, (d) etching, (e) anodization and pore widening, and (f) SAM-coupling to the AAO surface.

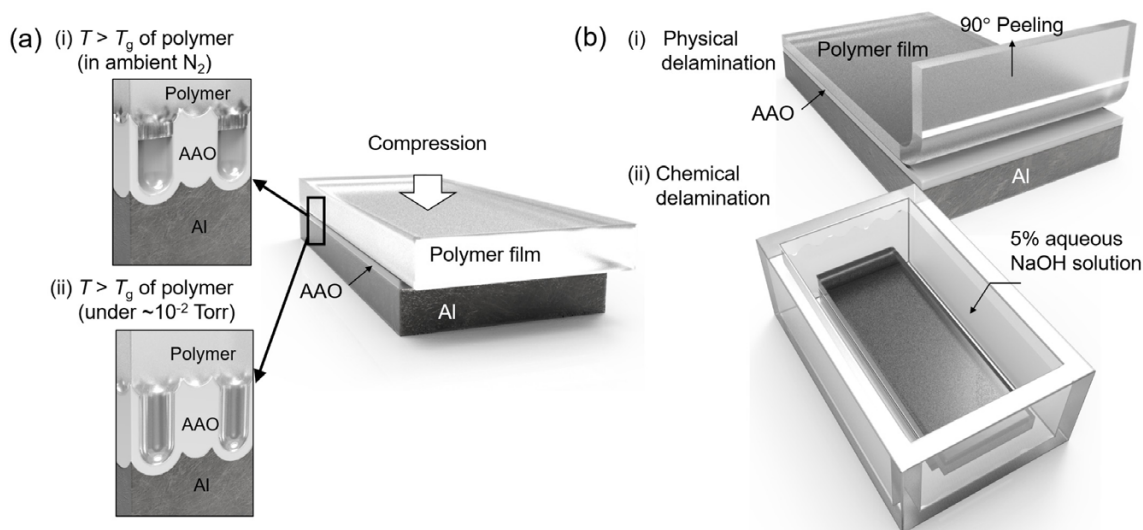


Figure 2. Scheme of (a) hot AAO pressing on a softened PS film (under $10^{-2}\sim 760$ Torr) and (b) two different ways of subsequently detaching the AAO mold from the polymer surface, *i.e.*, (i) physical delamination and (ii) etching.

into the AAO nanopores depends on the environmental vacuum pressure and temperature. Then, the treated polymer films were separated from the templates using either physical delamination (which will be discussed later) or chemical etching (as reported elsewhere) (Figure 2(b)). The Al and AAO layers were subsequently dissolved in 5% NaOH and 0.1 M aqueous H_3PO_4 (at 30 °C), respectively.²⁴

2.3. Characterization

The morphologies of the fabricated AAO layers and nano-textured polymer films were determined using scanning electron microscopy (SEM, JSM-7610F, JEOL) and atomic force microscopy (AFM, Multimode 8, Bruker). The WCA values of these textured polymer films were measured using a hand-made optical apparatus with a Nikon D7000 camera. The contact measurements for each sample were repeated at 10 or more different locations, and the resulting WCA values were averaged.

3. Results and Discussion

3.1. Porous AAO-assisted surface texturing on polymer films

Here, we successfully demonstrated that various nano-rod, -pile, -spike, and -fibril structures on polymer films could be developed with a porous AAO template. Porous AAO layers on an Al sheet or cylinder (as discussed later) were developed using a well-known two-step Al anodization process in a 0.1 M H_3PO_4 aqueous solution at 0 °C and 195 V.²³ The initial AAO pores were widened inside a 0.1 M H_3PO_4 solution (at 30 °C) until the value of D_p was about 200 nm. As shown in Figure 3, the second Al anodization induced hexagonally (HEX)-packed nanopores in the AAO layer, which were generated from a dimple-textured Al surface. Based on the top and cross-sectional SEM images, it was found that the AAO layer contained vertically-aligned nanopores with $D_p=200$ nm, $D_{inter}=500$ nm, and $H_p=1.6$ μ m.

To introduce various nano-textures on compression-molded polymer films, approximately 300- μ m-thick polymer films were placed on the AAO template, and both sides of the stacked polymer/AAO sample were sandwiched between glass slides (5 \times 7 cm², Corning Co.). The samples were gripped by a clamp with a spring constant of about 200 N m⁻¹ to apply compressive pressure. Then, they were transferred to a heating chamber and heated. At T_p of 160 °C, thermally-softened PS films in contact with the porous AAO layer were softened and either partially or com-

pletely filled into the porous columnar spaces with $D_p=200$ nm and $H_p=1.6$ μ m through vacuum pressure (Figure 2(a)). Finally, the AAO-imprinted PS films were either chemically or physically separated from the AAO templates (Figures 2(b)).

First, 300- μ m-thick PS films were imprinted using the AAO templates at $T_p=160$ °C with different vacuum pressures and were then separated from the templates. Figures 4(a)-(d), and 4(e) show SEM morphologies of the surface-textured PS films, resulting from chemical removal of the AAO templates. The textured PS films had HEX-packed nanostructures with an average height (H) range of <1 μ m to 1.6 μ m and an average domain spacing (Δ) of approximately 500 nm.²⁵ For the AAO-imprinted film containing an array of nano-piles (H of 400-450 nm, *i.e.*, an AR of 2.0-2.25) (Figures 4(a) and 4(b)), the corresponding AFM phase image clearly showed that each nano-pile had a topmost plateau region (Figure 4(c)), suggesting that a PS molten phase partially filled the AAO pores with $H_p=1.6$ μ m during hot pressing (at 160 °C in an N₂-atmosphere). As shown in Figure 4(f), the PS piles contained topmost concave points, indicating that the PS phase directly contacted the end side of the AAO pore during hot imprinting (Figure 4(f)). Note that, due to the physically-interlocking points between the PS and AAO layers, the embedded PS domains tended to be cut off during 90°-peeling separation when the AAO surface was untreated with a hydrophobic ODTS (as discussed later). In contrast, the longer PS piles ($D=200$ nm, $\Delta=500$ nm, and $H>2$ μ m, *i.e.*, AR>10) on the textured films tended to clump together and form collapsed aggregates after the AAO templates were chemically etched (Figure S3 in the SI).

3.2. Developing a strategy to obtain high-AR polymer nanostructures

It is known that clumping between standing cylindrical domains drastically decreases the real surface area on textured films, degrading the water repellency of the textured surface. In general, clumping occurs above a critical domain height (H_c), which can be determined using the following equation:²⁶

$$H_c = (E\Delta/W_{ad})^{1/3} \times (D/2) \quad (1)$$

where D , E , and W_{ad} are the average cross-sectional diameter of the domains, the modulus of the domains, and the energy of adhesion per unit area of contact between adjacent domains, respectively.

Based on Eq. (1), it was expected that the maximum H_c value for PS nano-piles aligned with $\Delta=500$ nm and $D=200$ nm

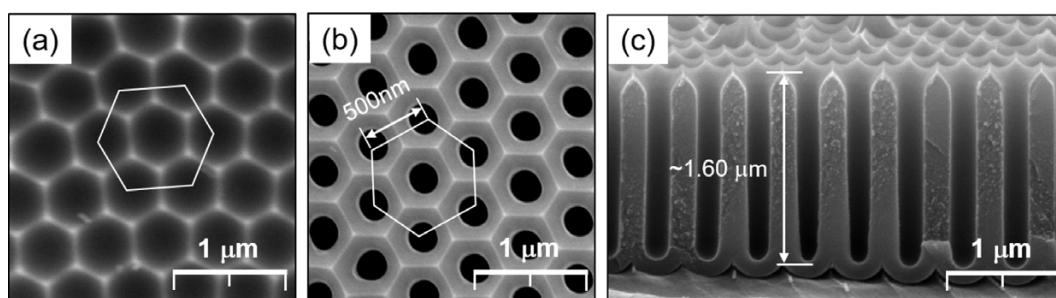


Figure 3. SEM micrographs of (a) the first anodized and sequentially-etched Al surface and (b, c) the second-anodized Al surface containing a porous AAO layer: (a, b) top view and (c) side view.

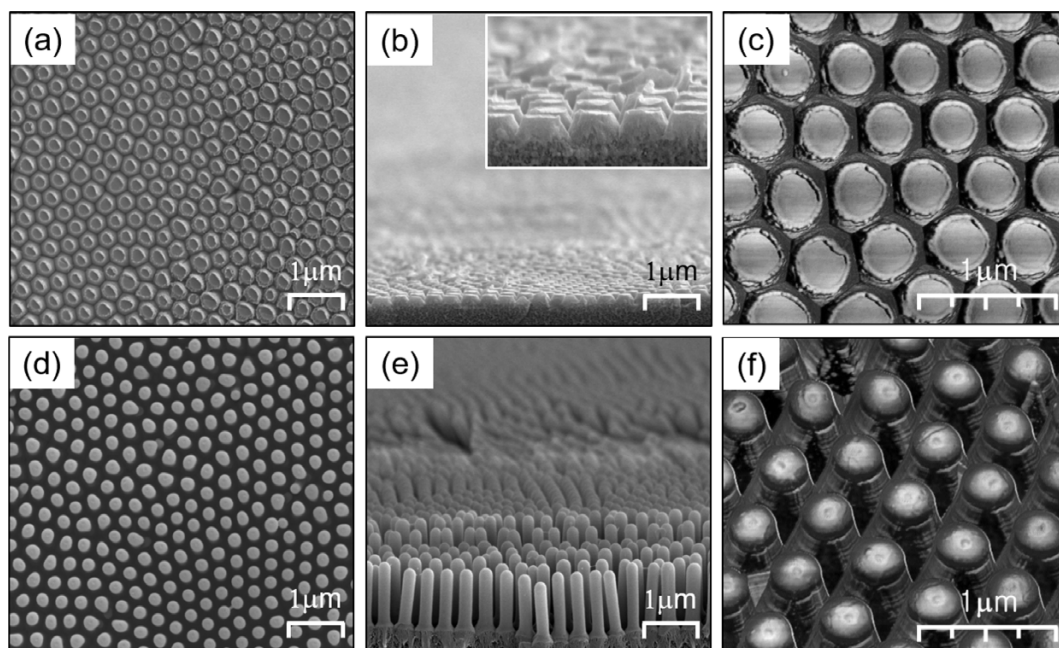


Figure 4. (a, b, d, e) SEM and (c, f) AFM micrographs of AAO-imprinted and chemically-separated PS films with different AR values: (a-c) 2.0-2.3 and (d-f) 7.5-8.5. (Note that the lateral and height dimensions in the AFM images are not accurate because it is difficult for an AFM tip with a polygonal geometry to accurately probe these textured surfaces³⁰).

(assuming $E=3.0$ GPa and $W_{ad}=80$ mJ m⁻²)²⁷ would be about 2.7 μ m. This also explains why thinner nano-piles with a high AR are difficult to be manipulated *via* chemical etching procedures without any clumping or collapse.

Here, we successfully demonstrated that the PS domains embedded inside of porous AAO layers can be deformed during

90° peel-off into variously-shaped structures, such as spikes or fibrils, by controlling the polymer-AAO interface and temperature. The T_g value of the 100 kDa PS used in this study was approximately 105 °C (Figure S2 in the SI). The PS domains embedded into AAO pores could be deformed and elongated even at 60 °C (below T_g).²⁸ This was related to the depression of the T_g in PS

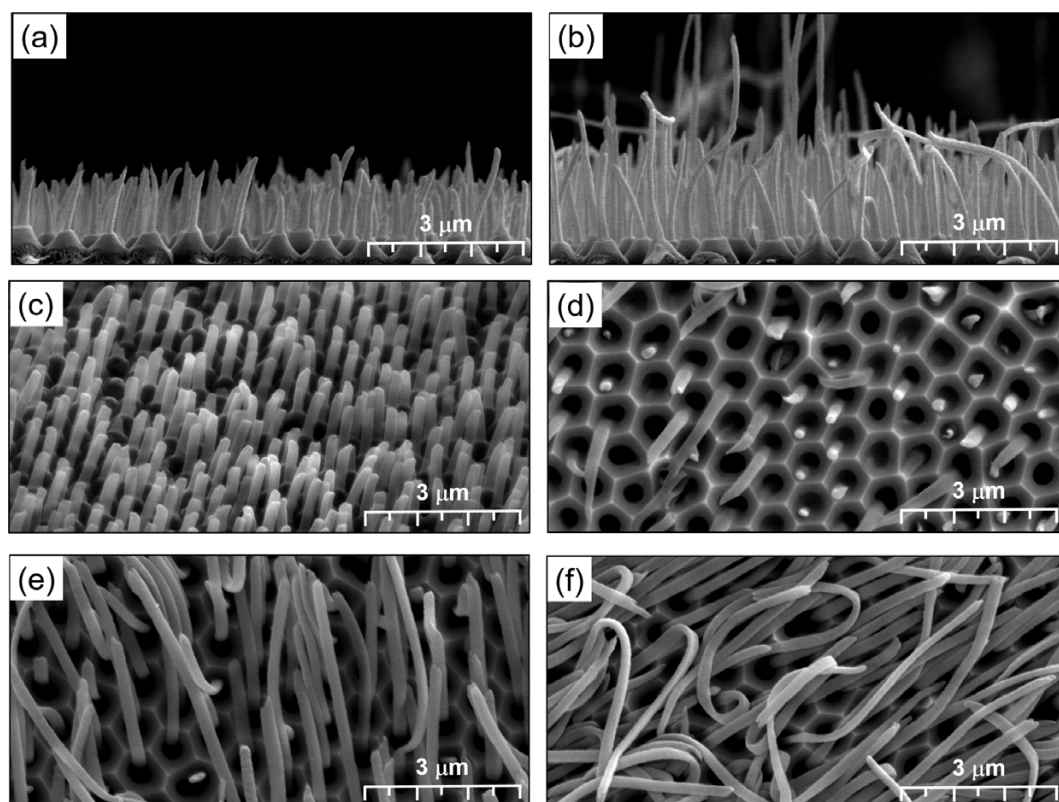


Figure 5. SEM micrographs of the (a-c) treated PS film and (d-f) AAO template after 90° peeling at different T_p : (a, d) 60, (b, e) 70, and (c, f) 80 °C.

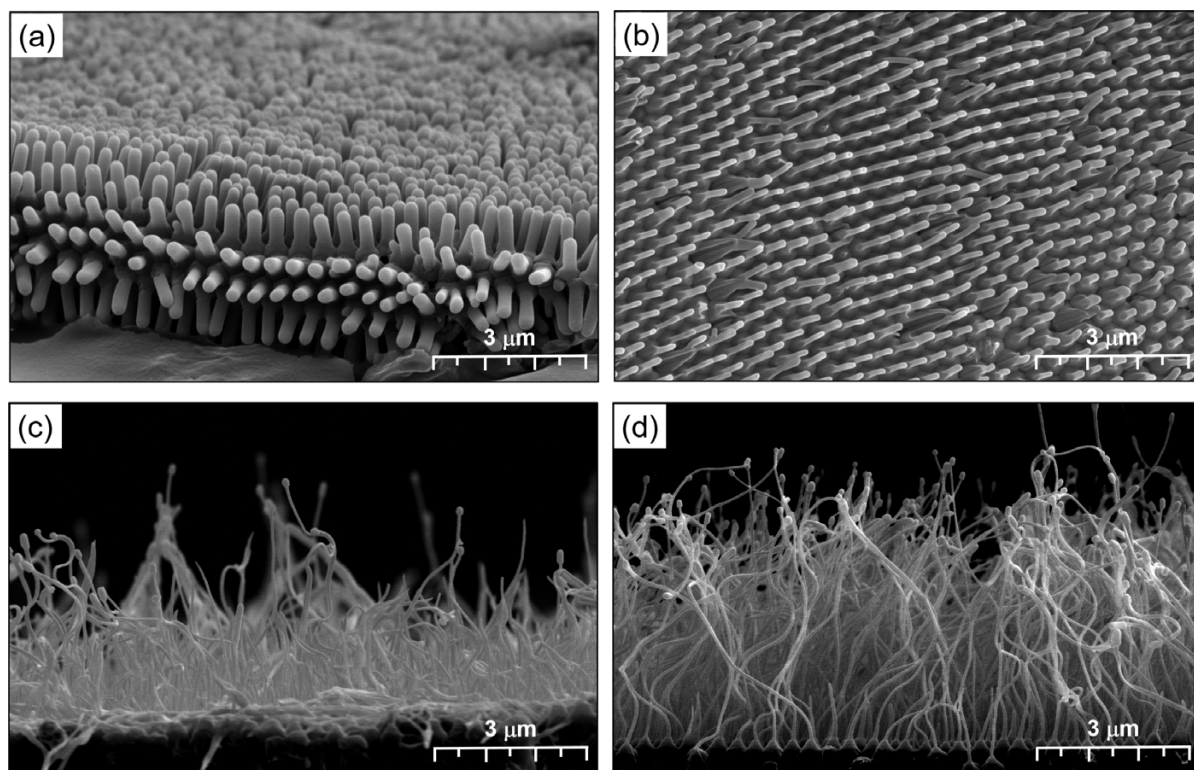


Figure 6. SEM micrographs of PS films imprinted with ODTS-treated AAO templates at different T_p : (a) room temperature, (b) 60, (c) 70, and (d) 80 °C (AR=110-130).

nano-domains, in comparison to that of bulk PS.²⁹

To separate the PS films from both the untreated and ODTS-treated AAO templates, a 90° peel-off method was conducted at a certain T_p , ranging from 60 to 80 °C, with a strain rate of approximately 5 mm s⁻¹ (Figure 2(b)). During peeling, the pore-embedded PS domains were deformed and sequentially elongated, depending on the T_p . Figure 5 shows SEM micrographs of the PS films separated from the untreated AAO templates and the separated AAO surfaces after 90° peeling at T_p =60, 70, and 80 °C, respectively. For the different T_p -treated samples, the pore-embedded PS domains did not undergo much elongation before failure, yielding PS nano-spikes with H =1.0-2.5 μm on the 60 °C-treated polymer films (Figure 5(a)). Particularly, the SEM morphology of the separated AAO surface clearly showed residues of the elongated PS phases after 90° peeling (Figure 5(d)). When the PS films were peeled at a T_p above 60 °C, the PS domains could be considerably deformed to yield high-AR fibrils. As shown in Figures 5(b)-(e), and 5(f), however, the SEM micrographs of the 70 °C- and 80 °C-treated samples revealed that the elongated PS domains were still cut off during 90° peeling, originating from mechanical interlocking of the polymer phase embedded into the AAO pores. For the 70 °C- and 80 °C-treated PS films, the AR values of the standing PS nanostructures increased up to 50 on the PS film, in comparison to the 60 °C-treated PS system with AR values ranging from 10-25).

Figure 6 shows SEM micrographs of the PS films textured with ODTS-treated AAO templates. The SEM morphologies of the PS films treated at T_p =60, 70, and 80 °C showed fibrillar structures that contained long necking regions without any failure, yielding a wide range of AR (H/D) values from 13 to 130. These

fibrillar structures were not obtained for the samples processed at room temperature. Additionally, these fibrillar ends were parabolic in shape, indicating traces of the original PS domains embedded into the AAO pores. Due to the benefit of the ODTS-treated AAO template, we successfully demonstrated that the embedded PS nano-domains could be highly elongated to achieve large surface areas for superhydrophobic film applications.

3.3. Structure-dependent water repellency on surface-textured polymer films

The water repellency of the untreated and surface-textured PS films was investigated by measuring the WCA values on typical PS films with nano-textures that processed different ARs (Figures 4-6). In comparison to the untreated PS film, which showed a WCA of 91±0.5°, the water repellency of the AAO-imprinted PS films was drastically enhanced with an increase in the AR of the polymer nanostructure on the film (Figure 7). In particular, the WCA was greater than 160° for the highly elongated hairy-textured PS film surface (Figure 6(d), AR>120).

3.4. Large-scale hydrophobic nano-texturing

The most practically important point of this study is that the two step surface texturing for polymer films (*i.e.*, hot AAO pressing and physical separation) can simply and reproducibly fabricate polymer films with controllable hydrophobicity. However, sheet-type AAO template-based imprinting has a size limitation and cannot be extended the surface nano-texturing process for large-scale polymer films.

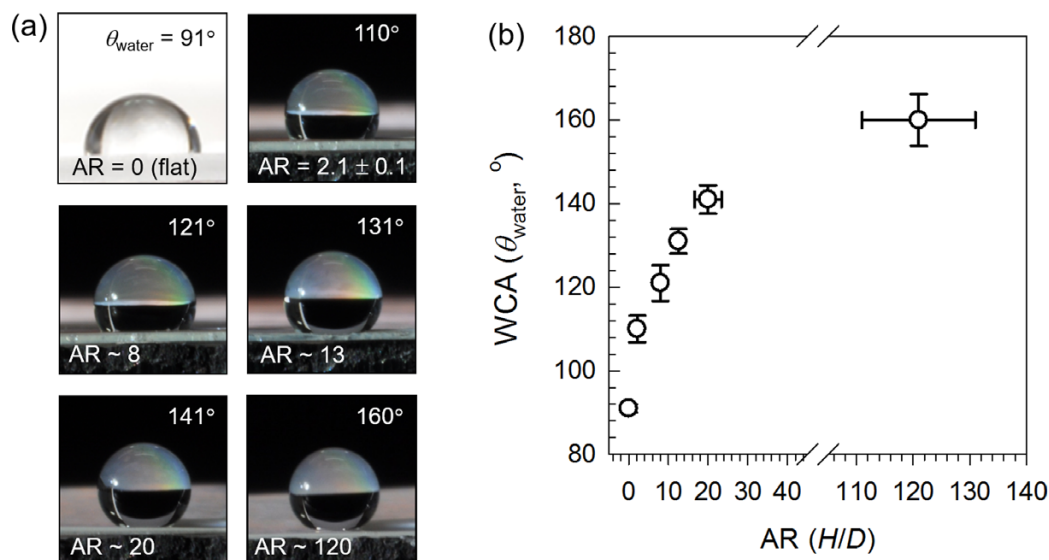


Figure 7. (a) Digital images of water droplets and (b) variations in the WCA on typical PS films textured with nanostructures that processed different ARs.

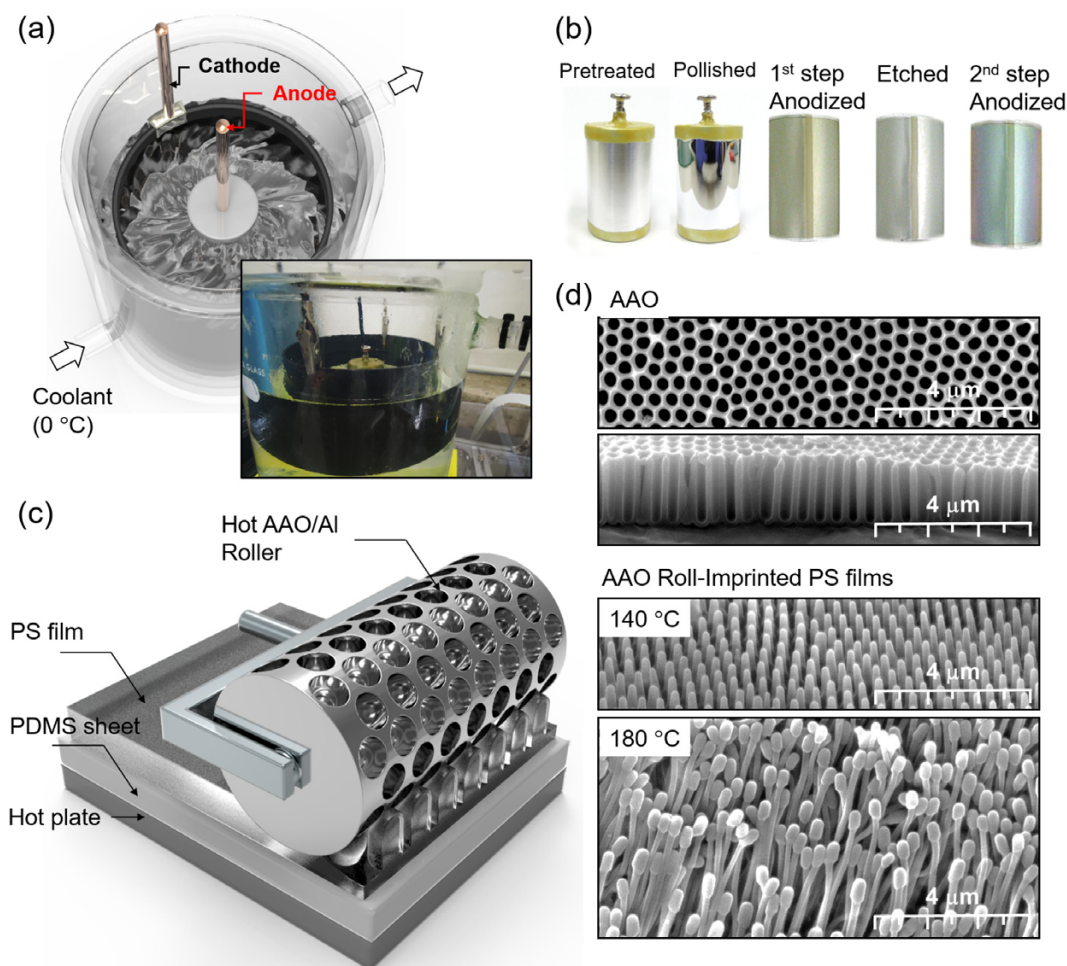


Figure 8. (a) Scheme of the anodization set-up with a circular tube-type carbon cathode and a highly-purified Al cylinder anode. (b) Typical appearance of the Al cylinder before and after each treatment. (c) Scheme of the one-step surface texturing of a polymer film with a porous AAO/Al cylinder heated to an elevated T_p . (d) SEM micrographs of the resulting AAO layer on the Al cylinder (top), and the resulting textured PS film after continuous roll pressing with the porous AAO/Al cylinder at T_p values of 140 and 180 °C (bottom).

Therefore, we designed an electrochemical set-up with a circular tube-type carbon cathode to anodize an Al cylinder (Fig-

ure 8(a)). The same procedure that was used with the Al sheets was used for an Al cylinder with a diameter of 3 cm and a height



Figure 9. Digital photographs of typical water droplets on (a) a rose petal, (b) a lotus leaf, and (c) a PS film roll-pressed at $T_p=180$ °C.

of 5 cm. Figure 8(b) shows the visible appearance of the Al cylinder after each treatment. After finishing the pore-widening step, the corresponding AAO layer on the Al cylinder showed vertical HEX-packed nanopores with a D_{ave} of 500 nm and an H of 1.5 μm (top images in Figure 8(d)). Similar to the sheet-type AAO imprinting process (Figure 2(b)), 300- μm -thick PS films were placed on a heating plate at 120 °C. These films were then roll-pressed using the cylindrical AAO template heated to 80 °C and continuously separated, as illustrated in Figure 8(c). The resulting textured PS films showed nano-piles or nano-hairs (bottom images in Figure 8(d)), depending on the T_p . As a result, we believe that the one-step hot AAO roll pressing of properly softened polymer films can produce a large-area films via a continuous procedure for hydrophobic polymer film texturing.

The WCA values on the roll-pressed PS film were comparable to those on representative superhydrophobic rose petals and lotus leaves. Water-sprayed droplets were mounted on all three surfaces. As shown in Figure 9, the roll-pressed PS film showed similar water repellent properties to both rose petals and lotus leaves, showing superhydrophobic characteristics with θ_{water} ranging from 145 to 160°.

4. Conclusions

We developed a facile approach for fabricating nano-hairs on polymer film surfaces. The formation of these structures was controlled using an AAO template with multi-level porous structures and nano-yielding processes. The AAO-treated polystyrene (PS) films showed various nano-textured surfaces, including vertically-standing domains (with similar spacing intervals of 500 nm). These domains changed from nano-pillars to nano-hairs, yielding a wide AR range from 1 to 130, depending on the viscoelastic response of the treated PS films during hot pressing and detachment of an AAO mold. WCA values of the nano-textured PS films dramatically changed from 91° to 160° with an increase in the AR. Using a similar hot pressing and physical detachment with an AAO-covered Al cylinder, we successfully demonstrated the fabrication of one-pot large-area nano-textured PS films that showed similar superhydrophobic character to rose petals and lotus leaves. We believe that this hot AAO roll pressing approach provides a simple, large-area, and versatile route to fabricate superhydrophobic polymer films.

Supporting information: Additional variation plots in depth and diameter of nanopores in AAO fabricated during the anod-

ization and pore widening, SEM and DSC. The materials are available *via* the Internet at <http://www.springer.com/13233>.

References

- (1) L. Feng, S. H. Li, Y. S. Li, H. J. Li, L. J. Zhang, J. Zhai, Y. L. Song, B. Q. Liu, L. Jiang, and D. B. Zhu, *Adv. Mater.*, **14**, 1857 (2002).
- (2) L. Feng, Y. A. Zhang, J. M. Xi, Y. Zhu, N. Wang, F. Xia, and L. Jiang, *Langmuir*, **24**, 4114 (2008).
- (3) X. M. Li, D. Reinhoudt, and M. Crego-Calama, *Chem. Soc. Rev.*, **36**, 1350 (2007).
- (4) P. Roach, N. J. Shirtcliffe, and M. I. Newton, *Soft Matter*, **4**, 224 (2008).
- (5) Y. W. Lee, S. H. Park, K. B. Kim, and J. K. Lee, *Adv. Mater.*, **19**, 2330 (2007).
- (6) M. S. Bell, A. Shahraz, K. A. Fichthorn, and A. Borhan, *Langmuir*, **31**, 6752 (2015).
- (7) B. Bhushan and Y. C. Jung, *J. Phys. Condens. Matter*, **20**, 225010 (2008).
- (8) E. Huovinen, J. Hirvi, M. Suvanto, and T. A. Pakkanen, *Langmuir*, **28**, 14747 (2012).
- (9) R. N. Wenzel, *Ind. Eng. Chem.*, **28**, 988 (1936).
- (10) A. B. D. Cassie and S. Baxter, *T. Faraday Soc.*, **40**, 546 (1944).
- (11) N. A. Patankar, *Langmuir*, **20**, 8209 (2004).
- (12) L. C. Gao and T. J. McCarthy, *Langmuir*, **22**, 2966 (2006).
- (13) A. Marmur, *Langmuir*, **20**, 3517 (2004).
- (14) D. Murakami, H. Jinnai, and A. Takahara, *Langmuir*, **30**, 2061 (2014).
- (15) V. A. Ganesh, H. K. Raut, and A. S. Nair, *J. Mater. Chem.*, **21**, 16304 (2011).
- (16) Y. Y. Yan, N. Gao, and W. Barthlott, *Adv. Colloid Interface*, **169**, 80 (2011).
- (17) E. Celia, T. Darmanin, E. T. de Givenchy, S. Amigoni, and F. Guittard, *J. Colloid Interface Sci.*, **402**, 1 (2013).
- (18) W. Lee, M. K. Jin, W. C. Yoo, and J. K. Lee, *Langmuir*, **20**, 7665 (2004).
- (19) D. Y. Lee, D. H. Lee, S. G. Lee, and K. Cho, *Soft Matter*, **8**, 4905 (2012).
- (20) C. H. Lim, S. Y. Han, J. D. Eo, K. Kim, and W. B. Kim, *J. Mech. Sci. Technol.*, **29**, 5107 (2015).
- (21) H. Masuda, K. Yada, and A. Osaka, *Jpn. J. Appl. Phys.*, **37**, L1340 (1998).
- (22) S. Z. Chu, K. Wada, S. Inoue, M. Isogai, Y. Katsuta, and A. Yasumori, *J. Electrochem. Soc.*, **153**, B384 (2006).
- (23) W. Lee and S. J. Park, *Chem. Rev.*, **114**, 7487 (2014).
- (24) K. Choi, S. H. Park, Y. M. Song, Y. T. Lee, C. K. Hwangbo, H. Yang, and H. S. Lee, *Adv. Mater.*, **22**, 3713 (2010).
- (25) W. K. Cho and I. S. Choi, *Adv. Funct. Mater.*, **18**, 1089 (2008).
- (26) B. Schubert, C. Majidi, R. E. Groff, S. Baek, B. Bush, R. Maboudian, and R. S. Fearing, *J. Adhes. Sci. Technol.*, **21**, 1297 (2007).
- (27) M. K. Chaudhury, *Mater. Sci. Eng. R.*, **16**, 97 (1996).
- (28) J. J. Wu and C. P. Buckley, *J. Polym. Sci., Part B: Polym. Phys.*, **42**, 2027 (2004).
- (29) J. L. Keddie, R. A. L. Jones, and R. A. Cory, *Europhys. Lett.*, **27**, 59 (1994).
- (30) Y. G. Kuznetsov and A. McPherson, *Microbiol. Mol. Biol. R.*, **75**, 268 (2011).